

---

## Size effects in Raman spectra of $\text{Sn}_2\text{P}_2\text{S}_6$ ferroelectrics

A.V.Gomonnai<sup>1</sup>, Yu.M.Vysochanskii<sup>2</sup>, Yu.M.Azhniuk<sup>1</sup>, I.P.Prits<sup>2</sup>,  
L.G.Romanova<sup>1</sup>, A.M.Solomon<sup>1</sup>

<sup>1</sup> Institute of Electron Physics, Ukr. Nat. Acad. Sci., 21Universytetska St.,  
Uzhhorod, 88000, Ukraine

<sup>2</sup> Uzhhorod National University, 46 Pidhirna St., Uzhhorod, 88000, Ukraine

Received 17.09.2001

### Abstract

Room-temperature Raman measurements of the  $\text{Sn}_2\text{P}_2\text{S}_6$  microcrystals are reported. The red shift, and broadening of the intense high-frequency first-order bands around  $380\text{ cm}^{-1}$  and in the range  $550\text{--}600\text{ cm}^{-1}$  with the microcrystal size decrease are observed. The possible mechanisms (phonon confinement, surface phonon scattering), responsible for these effects, are discussed.

**Keywords:** microcrystals, Raman scattering, phonon confinement, surface phonons.

**PACS:** 78.30.Hv, 63.20.Dj

### Introduction

Tin hexathiohypodiphosphate  $\text{Sn}_2\text{P}_2\text{S}_6$  crystal is a model semiconducting ferroelectric, where at 337 K a second-order structural phase transition  $P2_1/c \rightarrow Pc$  occurs [1]. The changes of the characteristic parameters of ferroelectric phase transitions with the size decrease from the bulk to microcrystals have been reported for oxygen-containing ferroelectrics:  $\text{PbTiO}_3$  [2, 3],  $\text{NaNO}_2$  [4],  $\text{KH}_2\text{PO}_4$  [4],  $\text{BaTiO}_3$  [5]. A special study is devoted to theoretical phenomenological approach to the size effect on the phase transitions in such ferroelectrics [6] It should be also noted that semiconductor microcrystalline materials, synthesized in different inorganic and organic matrices, are extensively studied by spectroscopic techniques due to the quantum-size effects related to spatial confinement of charge carriers [7]. Therefore it seems interesting to investigate specific features revealed in the optical properties of the semiconductor and ferroelectric  $\text{Sn}_2\text{P}_2\text{S}_6$  with the decrease of the

crystal size, using the Raman scattering as an effective tool for vibrational spectroscopy.

### Experimental procedure and results

To investigate  $\text{Sn}_2\text{P}_2\text{S}_6$  microcrystals of different average size ( $\sim 50\text{ }\mu\text{m}$  and  $\sim 5\text{ }\mu\text{m}$ ) were used, being obtained by different techniques. The bigger ( $\sim 50\text{ }\mu\text{m}$ ) microcrystals were prepared by milling  $\text{Sn}_2\text{P}_2\text{S}_6$  single crystals, grown by Bridgman technique with subsequent sieving. Smaller ( $\sim 5\text{ }\mu\text{m}$ ) microcrystals were prepared by the interaction of  $\text{SnCl}_2$  and  $\text{Li}_2\text{P}_2\text{S}_6$  water solutions with subsequent purification of the precipitate by centrifuging, evaporation, washing, filtering and vacuum drying [8].

Both types of microcrystals were incorporated into a polyvinyl alcohol (PVA) matrix by dispersion in aqueous solution of the PVA with average molecular mass 70000 and average content of acetate groups 1.4 mass %, subsequent thermal treatment at 363 K during 3 h, storage at room temperature during 24 h and

drying. The concentration of microcrystals in the obtained films varied from 1 to 10 mass %.

The structure of the obtained samples was checked by X-ray diffraction analysis performed by using a standard Bragg–Brentano scheme. The recorded diffractograms of the  $\text{Sn}_2\text{P}_2\text{S}_6$  microcrystals embedded in the PVA matrix, the PVA matrix itself and polycrystalline  $\text{Sn}_2\text{P}_2\text{S}_6$  are shown in Fig. 1. The comparison of the curves in the figure with the diffractogram

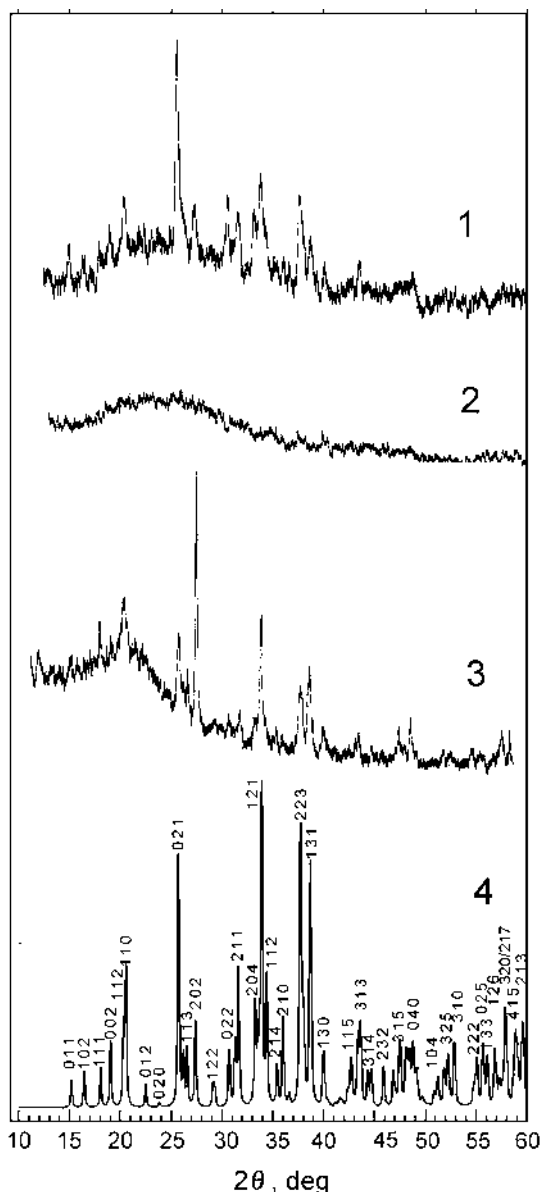


**Fig. 1.** X-ray diffraction pattern of  $\text{Sn}_2\text{P}_2\text{S}_6$  microcrystals embedded in PVA matrix (1), PVA matrix itself (2), polycrystalline  $\text{Sn}_2\text{P}_2\text{S}_6$  (3) compared with the computations based on the data of [10] (4).

calculated by using the structural site positions of  $\text{Sn}_2\text{P}_2\text{S}_6$  [9, 10] clearly shows the presence of  $\text{Sn}_2\text{P}_2\text{S}_6$  crystalline phase in the prepared film samples.

The Raman spectra of  $\text{Sn}_2\text{P}_2\text{S}_6$  microcrystals ( $\lambda=632.8$  nm, LOMO DFS-24 spectrophotometer), recorded at room temperature, are shown in Fig. 2 along with the bulk crystal spectrum.

Bulk  $\text{Sn}_2\text{P}_2\text{S}_6$  crystals are known to possess a rich Raman spectrum, its polarization features and temperature behaviour having been extensively studied in [11–13]. As our measurements have shown, the Raman spectra of  $\text{Sn}_2\text{P}_2\text{S}_6$  microcrystals reproduce the unpolarized Raman spectrum of the bulk material, especially in the frequency range 160–300  $\text{cm}^{-1}$  where the deformational S-P-S modes, are observed, and in the interval 550–600  $\text{cm}^{-1}$  corresponding to the internal vibrations of  $(\text{P}_2\text{S}_6)^{4-}$  anionic structural groups (Fig. 2).

The convenient spectral position and high intensity of P–P bond vibration of  $(\text{P}_2\text{S}_6)^{4-}$  anions enabled its frequency, halfwidth and lineshape to be chosen for the detection of size-related effects in the Raman spectrum. The corresponding part of the Raman spectrum is shown in Fig. 3. We observed the P–P band frequency to decrease from 381.4  $\text{cm}^{-1}$  in the bulk samples to 380.2  $\text{cm}^{-1}$  (50- $\mu\text{m}$  microcrystals) and 379.9  $\text{cm}^{-1}$  (5- $\mu\text{m}$  microcrystals), accompanied by the growth of the band halfwidth from 5  $\text{cm}^{-1}$  (bulk material) to 8  $\text{cm}^{-1}$  (50- $\mu\text{m}$  size) and 11  $\text{cm}^{-1}$  (5- $\mu\text{m}$  size) and lineshape transformation.

The size-induced variation of the Raman band parameters is also revealed for the internal vibrations of  $(\text{P}_2\text{S}_6)^{4-}$  anion in the range of 550–600  $\text{cm}^{-1}$  (Fig. 4) where in the bulk  $\text{Sn}_2\text{P}_2\text{S}_6$  crystals five  $A'$  phonon bands are superimposed at room temperature. The experimentally observed spectra were simulated by a set of five Gaussian contours (dashed lines). The peak frequencies, corresponding to the best fit of the experiment, are listed in Table 1.

**Table 1.** Raman peak frequency positions in the  $(P_2S_6)^{4-}$  anion internal vibration frequency range for bulk and microcrystalline  $Sn_2P_2S_6$

Band No.	Bulk sample	$\sim 50 \mu m$ microcrystals	$\sim 5 \mu m$ microcrystals
1	$556 \text{ cm}^{-1}$	$555 \text{ cm}^{-1}$	$541 \text{ cm}^{-1}$
2	$557 \text{ cm}^{-1}$	$556 \text{ cm}^{-1}$	$551 \text{ cm}^{-1}$
3	$568 \text{ cm}^{-1}$	$565 \text{ cm}^{-1}$	$555 \text{ cm}^{-1}$
4	$577 \text{ cm}^{-1}$	$575 \text{ cm}^{-1}$	$566 \text{ cm}^{-1}$
5	$590 \text{ cm}^{-1}$	$586 \text{ cm}^{-1}$	$583 \text{ cm}^{-1}$

As seen from Fig. 4 and Table 1, in the discussed frequency range the same general trend of the Raman peak frequency decrease with the reduction of the crystal size is clearly observed, in spite of the considerable number of the superimposing Raman bands.

There are several factors which can generally be responsible for the phonon band frequency and width dependence on the microcrystal size. While in the bulk crystal the

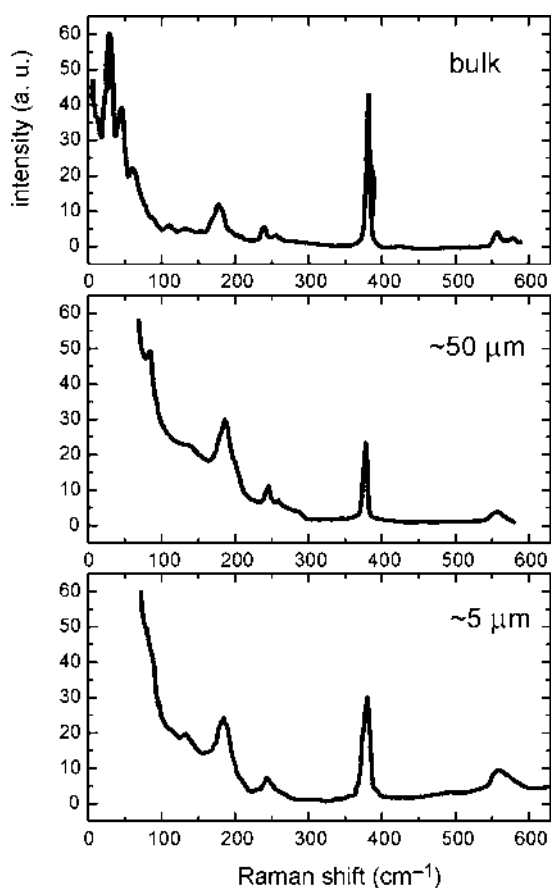


**Fig. 2.** Raman spectra of  $Sn_2P_2S_6$  bulk and microcrystals at room temperature.

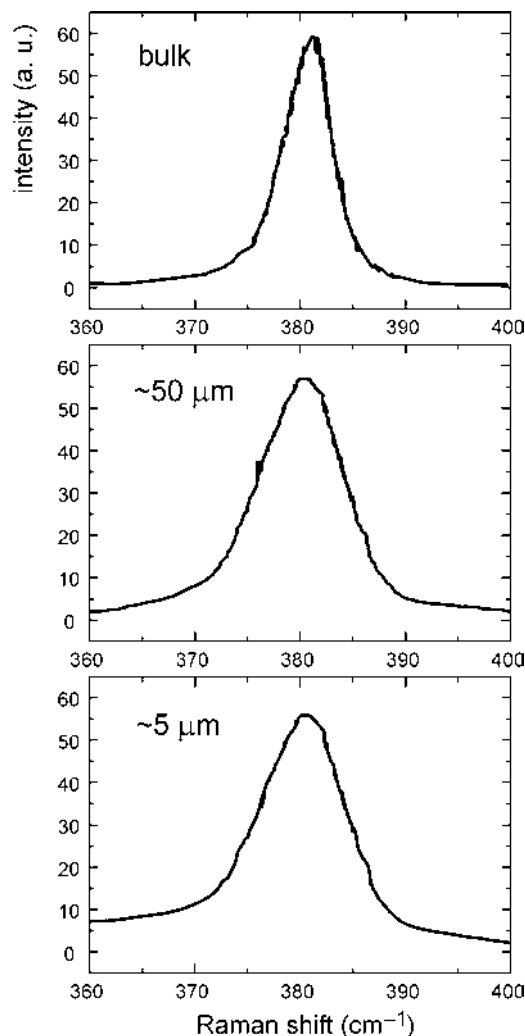


**Fig.3.** Part of the Raman spectra, corresponding to P–P bond vibration, for  $Sn_2P_2S_6$  bulk and microcrystals.

phonon eigenstate is a plane wave and the wave vector selection rule of the first-order Raman scattering requires the phonon wave vector  $q$  to be near-zero. In microcrystals the spatial correlation function of the phonon becomes finite due to its confinement, and hence the  $q \approx 0$

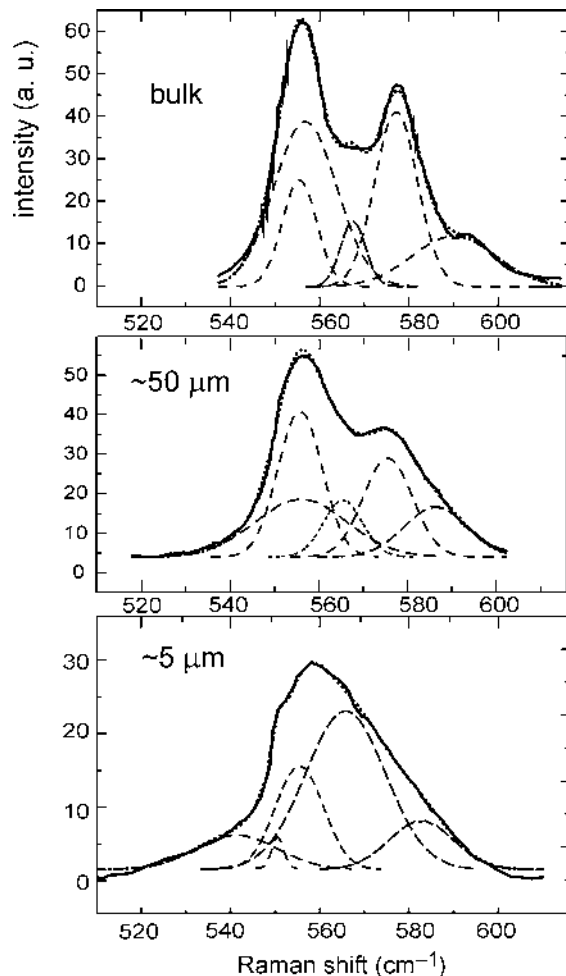


**Fig. 4.** Part of the Raman spectra, corresponding to  $(\text{P}_2\text{S}_6)^{4-}$  anion internal vibrations, for the  $\text{Sn}_2\text{P}_2\text{S}_6$  bulk and microcrystals: solid line – experimental spectrum, dotted line – superposition of the Gaussian contours, each of them shown by a dashed line.

is relaxed. In general, since the optical phonon dispersion curves of the bulk crystal show the frequency  $\nu$  to be a decreasing function of the wave vector  $q$ , the red shift and broadening of the first-order Raman bands are observed, the corresponding results for Si, III-V and II-VI microcrystals having been reported [14–16]. Besides, in ionic microcrystals surface phonon modes can be observed, growing intensively with the microcrystal size decrease due to the increased surface-to-bulk contribution ratio. The surface phonon modes in microcrystals can reveal as additional features with frequencies below those to the corresponding bulk LO phonon maxima [14, 16]. In most cases the

contributions from both effects cannot be separated and are observed as general red shift and broadening of the Raman bands. This, in particular, applies to our case of  $\text{Sn}_2\text{P}_2\text{S}_6$  microcrystals, since the grain size is not very small. Besides, the discussed effects can be encumbered by the possible downward shift of the Raman band frequencies due to the size-induced decrease of the phase transition temperature.

## Conclusions

Raman measurements of the  $\text{Sn}_2\text{P}_2\text{S}_6$  microcrystals have revealed a noticeable dependence of the frequencies and halfwidths of the most intensive high-frequency first-order bands, corresponding to the P–P bond vibrations (around  $380\text{ cm}^{-1}$ ) and internal vibrations of  $(\text{P}_2\text{S}_6)^{4-}$  anion in the range of  $550\text{--}600\text{ cm}^{-1}$  on the microcrystal size. The observed red shift, and broadening of the discussed bands are related to the selection rules relaxation due to phonon confinement in the microcrystals and/or surface phonon modes due to the increase of the surface-to-volume contribution ratio with the microcrystal size decrease.

**Acknowledgment.** The authors are grateful to V.B.Cajipe for presenting the part of the  $\text{Sn}_2\text{P}_2\text{S}_6$  microcrystal powders used for the experiments.

## References

1. Vysochanskii Yu.M. and Slivka V.Yu., *Uspekhi Fiz. Nauk* **162**, (1992) 139 (in Russian).
2. Ishikawa K., Yoshikawa K. and Okada N., *Phys. Rev. B* **37** (1988) 5852.
3. Zhong W.I., Jiang B.I., Zhang P.L., Ma J.M., Cheng H.M., Yang Z.H. and Li L.X., *J. Phys.: Condens. Matter* **5** (1993) 2619.
4. Colla E.V., Fokin A.V., Koroleva E.Yu., Kumzerov Yu.A., Vakhrushev S.V. and Savenko V.N., *Nanostructured Materials* **12** (1999) 963.
5. Uchino K., Sadanaga E. and Hirose T., *J.*

- Amer. Ceram. Soc. **72** (1989) 1555.
6. Zhong W.L., Wang Y.G., Zhang P.L. and Qu W.D., Phys. Rev. B **50** (1994) 698.
  7. Gaponenko S.V., Fiz. Tekhn. Poluprovodn. **30** (1996) 577 (in Russian).
  8. Bourdon X. and Cajipe V.B., J. Sol. St. Chem. **141** (1998) 290.
  9. Dittmar G. and Schaefer H., Z. Naturforsch. B. **29** (1974) 312.
  10. Voroshilov Yu V, Vysochanskii Yu.M., Grabar A.A., Potori M.V., Prits I.P., Rizak V.M., Sejkovskaja.L.A., Slivka V.Yu. and Vatsenko A.V., Ukr. Fiz. Zh. **35** (1990) 71 (in Russian)
  11. Vysochanskii Yu.M., Slivka V.Yu., Voroshilov Yu.V., Gurzan M.I. and Chepur D.V., Fiz. Tverd. Tela. **21** (1979) 2402 (in Russian).
  12. Gomonnai A.V., Vysochanskii Yu.M., Grabar A.A. and Slivka V.Yu., Fiz. Tverd. Tela. **23** (1981) 3623 (in Russian).
  13. Gomonnai A.V., Vysochanskii Yu.M. and Slivka V.Yu., Fiz. Tverd. Tela. **24** (1982) 1068 (in Russian).
  14. Hayashi S., Sol. State Commun. 56 (1985) 375.
  15. Fauchet P.M. and Campbell I.H., Sol. State Commun. 58 (1986) 739.
  16. Roy A. and Sood A.K., Phys. Rev. B **53** (1996) 12127